Available online at www.sciencedirect.com
ScienceDirect
International Journal of Solids and Structures 44 (2007) 5774–5795
INTERNATIONAL JOURNAL OF SOLIDS AND STRUCTURES
www.elsevier.com/locate/ijsolstr

Dimensionless parameters in symmetric double lap joints: An orthotropic solution for thermomechanical loading

Peter A. Gustafson, Arnaud Bizard, Anthony M. Waas *

Department of Aerospace Engineering, University of Michigan, Ann Arbor, MI 48109, USA

Received 13 October 2006; received in revised form 25 December 2006
Available online 30 January 2007

Abstract

Two thermomechanical analytical models are developed for orthotropic double lap joints with a view to identifying key dimensionless parameters that describe the behavior of the joint under combined thermal–mechanical loads. The solutions, based on the principle of virtual work, differ in the complexity of the assumed stress field. The first solution is similar to Volkersen [Volkersen, O., 1938. Die niektraftverteilung in zugbeanspruchten mit konstanten laschenquerschritten. Luftfahrtforschung 15, 41–47] with the addition of orthotropic and thermal effects. The second solution, extending the work of Davies [Davies, G.A.O., 1982. Virtual Work in Structural Analysis, John Wiley & Sons, New York] captures the peel stress as well as the traction free boundary condition at the adhesive edge. Relevant non-dimensional parameters are identified in terms of geometric, material, and load quantities. A dimensionless load ratio is identified which dictates the shape of the stress distribution. This ratio can also be used to quickly determine the dominant loading mechanism. Dimensionless stress plots are presented for representative lap joints.

Keywords: Lap joint; Adhesive bond; High temperature; Composite; Thermal expansion; Non-dimensional parameters

1. Introduction

The use of composite materials continues to increase in the aerospace industry, which places an increasing importance on the ability of designers to properly specify the performance of bonded structural joints. Due to specific strength, specific stiffness, and efficient load distribution and load transfer, recent high profile aircraft and spacecraft have featured bonded joints. New epoxies and adhesives have shown great promise to expand the temperature range over which structural fiber reinforced polymer composites are used. These materials provide an opportunity to replace specialized, non-structural thermal protection with integrated composite systems capable of carrying structural load over a range of temperature extremes. Consequently, temperature resistant composite structures and bonded joints will be used in increasing quantities. In addition to the harsh operating environments, the processing temperatures for these specialized epoxies and adhesives are also quite

* Corresponding author.
E-mail address: dcw@umich.edu (A.M. Waas).

0020-7683/$ - see front matter
doi:10.1016/j.ijsolstr.2007.01.025

Nomenclature

t_κ	material thicknesses of component κ (m)
l	lap length (m)
x	lap coordinate measured from the left edge (m)
y	lap coordinate measured from the lower edge (m)
$\sigma_{\kappa 11(x)}$	longitudinal stress in component κ (Pa)
$\sigma_{\kappa 22(x,y)}$	transverse stress in component κ (Pa)
$\tau_{\kappa 12(x)}$	shear stress in component κ (Pa)
$E_{\kappa ii}$	orthotropic engineering moduli of component κ (Pa)
G_{b12}	shear modulus of the adhesive (Pa)
$E_{p^{[0]}}$	Young's moduli of the end posts (Pa)
$v_{\kappa ij}$	Poisson's ratios of component κ
$\alpha_{\kappa ii}$	orthotropic thermal expansion coefficient of component κ ($^\circ C^{-1}$)
P	mechanical load applied to joint, per unit depth (N m^{-1})
ΔT	temperature change from reference temperature (°C)
F	mechanical load carried by an end post (N)
c_0, d_0	coefficients of assumed stress distribution (N)
c_1, d_1	coefficients of assumed stress distribution (N m^{-1})
ψ_P	mechanical load parameter (N m^{-4})
ϕ_P	mechanical load parameter (N m^{-6})
ψ_T	thermal load parameter (N m^{-4})
ϕ_T	thermal load parameter (N m^{-6})
ω	system parameter (m^{-1})
β	system parameter (m^{-2})
γ	system parameter (m^{-4})
$\bar{x}$	dimensionless coordinate $\frac{x}{l}$ measured from the left edge of the adhesive
$\overline{\omega}$	dimensionless system parameter
$\overline{\beta}$, $\overline{\gamma}$	dimensionless system parameters
$\overline{\lambda}_1$, $\overline{\lambda}_3$	dimensionless system parameters
$\overline{\sigma}_{\kappa 11(x)}$	dimensionless longitudinal stress in component κ
$\overline{\sigma}_{\kappa 22(x,y)}$	dimensionless transverse stress in component κ
$\overline{\tau}_{\kappa 12(x)}$	dimensionless shear stress in component κ
$\overline{\overline{\sigma}}_{a11(x)}$	normalized dimensionless longitudinal stress in component a
$\overline{\psi}_P$, $\overline{\phi}_P$	dimensionless mechanical load parameters
$\overline{\psi}_T$, $\overline{\phi}_T$	dimensionless thermal load parameters
$\overline{\phi}_{aR}$, $\overline{\phi}_{cR}$	dimensionless thermal to mechanical load ratios
$\overline{\phi}_{\text{total}}$	dimensionless total load parameter
$\overline{\overline{\phi}}_P$	dimensionless mechanical load fraction
$\bar{a}, \bar{b}, \bar{A}, \bar{B}, \bar{C}, \bar{D}$	dimensionless coefficients
$\bar{\bar{a}}, \bar{\bar{b}}, \bar{\bar{A}}, \bar{\bar{B}}, \bar{\bar{C}}, \bar{\bar{D}}$	dimensionless coefficients
$\hat{\sigma}_{\kappa 11(x)}$	longitudinal virtual stress in component κ
$\hat{\sigma}_{\kappa 22(x,y)}$	transverse virtual stress in component κ
$\hat{\tau}_{\kappa 12(x)}$	shear virtual stress in component κ
[]	the *or* operator, i.e. [13] is 1 *or* 3 (no sum)
κ	$\kappa = [abc]$ (no sum) representing central adherend (a), adhesive (b), and outer adherend (c), respectively
ii	$i = [123]$ (no sum)
ij	$i,j = [123]$ where $i \neq j$ (no sum)

high. As a result, the materials carry a significant risk of adverse stress fields caused by differential thermal expansion, even at room temperature.

It has been claimed that approximately 70% of structural failures are initiated in joints (Her, 1999), therefore great attention must be paid to proper design of joints. Engineers have long recognized that adhesively bonded joints reduce stress concentrations associated with mechanical fasteners through a more even distribution of the transmitted load. As the adhesives available for bonding have improved, the use of bonded joints has enhanced or replaced the use of traditional mechanical fasteners in high performance aircraft. Confidence in such joints has grown with accumulated usage, as reflected in the use of bonded joints in the joint strike fighter and the long range strike aircraft (Zhang et al., 2006; Bednarcyk et al., 2006). Additionally, the use of adhesively bonded composite joints has expanded into the automotive industry. [1]

Despite increased usage, the design of joints is often carried out in an ad-hoc fashion, relying heavily on physical testing and empirical models. If the role of temperature resistant composites is to expand, their use must be supported by an improved understanding of bonded joints. Further research is needed to expand modeling capability for bonded joints, as well as to determine the mechanical response of material systems. It is also important to transfer research level models into the product development environment.

The main objective of the present paper is to introduce appropriate non-dimensional parameters that govern joint performance under combined thermal-mechanical loads. These parameters can be used to quickly identify the effects of material orthotropy and joint geometry on joint performance. Two thermomechanical models are presented for the symmetric double lap joint, a joint commonly used in the aerospace industry. The first model, referred to as the shear only model (SO), can be considered a thermomechanical extension to Volkersen (1938). The joint response is calculated based on the assumption of a very simplified stress field. The solution provides a basic method for determining the effects of the key parameters on the global shear response of the joint. A second model, more complicated than the first due to the inclusion of shear and peel stress in the adhesive, extends the first solution. This extension allows for the calculation of peel stresses while satisfying the traction free adhesive edge condition. It will therefore be referred to as the shear-peel model (SP). To establish the utility of these models, both models are compared to a reference finite element (FE) model. Finally, both models are shown to contain an identical dimensionless ratio of thermal to mechanical loads, which easily identifies the relative importance of these loading types to a joint design. The extension of the main findings of this work to a single lap joint is the subject of a separate investigation.

2. A brief summary of double lap joint analytical models

Analytical solutions to the bonded joint have been introduced previously. First among them Volkersen (1938), followed by Goland and Reissner (1944), both of which presented solutions to the single lap joint. In addition, their have been many authors (an incomplete list includes: Her (1999), Hart-Smith (1973b), Pippiatt (1974), Renton and Vinson (1975), Allman (1977), and Yang et al. (2004)) who have proposed models for single lap joints. (Additionally, summaries were provided by Benson (1966) and Adams et al. (1997).) Of greater interest to this work, several authors have addressed double lap joints including Her (1999), Hart-Smith (1973a), Gilibert and Rig olot (1988), Sen and Jones (1980a,b), Mendels et al. (2000), and Mortensen and Thomsen (2002b). The latter of these and its descendents are analytical derivations of the governing equations, though the lack of an available closed form solution causes the evaluation to be numerical. The double lap solution of Davies (1982) inspired the SP analysis of the current work. Though intended for single lap joints, the work of Volkersen (1938) could be used for double lap joints with only slight modification.

There are several important issues present in bonded lap joints which have commonly been neglected or considered irrelevant to the problems that were solved. Three of these issues will be considered in the present models. First, in an idealized lap joint, the edge of the adhesive is a traction free surface. The average shear stress builds to an extremum over a small boundary region. Though this is captured in some models, it is not captured in the frequently cited work of Goland and Reissner (1944), nor its descendents. For example, in the double lap solution of Hart-Smith (1973a), inappropriate interpretation of the model could lead to a

[1] Composites News International, *Ashland Pliogrip Adhesive Bonds Roofs To Two BMW Sports Sedans*, Jan 20, 2006.

conclusion that the shear stress is maximized at the edge of the adhesive, instead of being zero. Several authors have presented double lap joint models which capture the traction free boundary condition, however the derived solutions are either numerical as in the case of Sen and Jones (1980a,b), or the governing equation is a differential equation of very high order as in the case of Whitney (1997). Though the models which do not resolve the traction free edge condition can nevertheless be correctly interpreted by an analyst (as is required for the SO solution presented in this work), it is advantageous and analytically more pleasing to satisfy this boundary condition when possible. It was noted by Benson (1966) that a minimum 4th order differential equation (of the field displacement) is required to capture the traction free surfaces. The SP of the present work has such a differential equation, and the direct advantage over the SO solution is the ability to calculate peel stress.

A second issue is a general lack of accounting for the anisotropic material behavior of the joint constituents (adherends and adhesive) in the available analytical solutions of the literature. Exceptions exist, for example Erdogan and Ratwani (1971) and Delale et al. (1981), though these are neither double lap joint models nor are *all* constituents anisotropic in these studies. This lack of anisotropy in a model is particularly a concern when considering laminated composite materials, since transverse properties are often significantly lower than in-plane properties for a given laminate Hart-Smith, 1973a. Also, since high temperature curing cycles are frequently needed for temperature resistant materials, prudence dictates that anisotropic material behavior should be included in thermomechanical analytical models. This need has been recognized and is an active area of current research. Recent work includes Mortensen and Thomsen (2002a,b), Zhang et al. (2004, 2005, 2006), Yarrington et al. (2005), and Bednarcyk et al. (2006). In contrast to the listed contributions, the present work provides closed-form, parametric solutions with orthotropic material properties in all constituents. The parametric nature of these solutions reveal previously unrecognized insights into joint performance.

A third issue is found at the edge of the adhesive, this time at the corner interfaces between the adherends and the adhesive. In these locations, geometric discontinuities cause unbounded stress concentrations in any solution based on linear elastic continuum mechanics Kilic et al., 2004. Though non-linear material response might ensure that the stress remains finite Zhang et al., 2004, the peak stresses at the corners are very dependent on the specific geometry and material behavior. The possible effects are not considered in the analytical models presented in this work, since this aspect of the joint requires different modeling strategies that employ ideas rooted in fracture mechanics. However, the geometric discontinuity affects the FE models which are presented for comparison, and therefore must be considered when evaluating the results. Specifically, it is important to recognize that the reference linear elastic FE model in this work is not a correct solution at the corners. It is flawed at these geometric discontinuities, and the stress concentrations will not converge with increasing element density. Therefore, direct comparisons between the FE solution and the present analytical work are only meaningful away from the singular corners. However, in contrast to FE based solutions, the analytical models provided in this work allow for meaningful comparison between different joint designs. The models have no mesh dependence, and the predicted stresses remain finite.

Finally, temperature effects were not considered in most of the analytical double lap joint models currently available. The authors are aware of the work of Hart-Smith (1973a), Chen and Nelson (1979), Vinson and Zumsteg (1979), and Adams et al. (1992) who included thermal effects in their solutions. Hart-Smith provided an excellent double lap solution which included thermal loading. However, the work focused more on material non-linearities and did not capture the traction free boundary condition (Hart-Smith, 1973a). The bonded joint solutions of Chen and Nelson (1979) include thermal expansion, however the materials are isotropic and no double lap analysis is included. The contributions of Vinson and Zumsteg (1979) include a composite thermal-mechanical solution of a double lap joint. However, the solution is difficult to evaluate in that it requires the solution of 18 simultaneous boundary conditions and can only be reasonably solved numerically. Qualitative assessments cannot be made since no plots of the predicted stresses were provided. Finally, the work of Adams et al. (1992) focused on thermal loading in lap joints, however the subject matter was single lap joints and the solutions were FE based. In the following sections of this paper, two thermomechanical analytical models of the double lap joint are presented and appropriate non-dimensional parameters are identified. These models are shown to be very useful in evaluating the thermo-mechanical performance of the joint.

3. Analytically derived stress field in a double lap joint including thermal expansion

3.1. A model which assumes the adhesive carries shear stress only

A schematic of a double lap joint is shown in Fig. 1. In this work, a symmetric geometry is assumed, and two solutions will be proposed. The first solution will assume that the stress field varies only along the direction of loading. The adherends are assumed to carry longitudinal normal stress only, and the adhesive is assumed to carry shear stress only. Due to symmetry, the bending moments present in the joint are assumed to be negligible. Therefore, bending of adherends is not included. Under these assumptions, the stress field is a function of x only. Thermal expansion is assumed to be linear with temperature. Plasticity, creep, and other non-linearities of the constituents are ignored, though it is likely that they could be significant Hart-Smith, 1973a. Under these assumptions and assuming plane strain deformation, the constitutive equations for material κ are governed by:

$$\begin{Bmatrix} \epsilon_{\kappa 11}(x) \\ \epsilon_{\kappa 22}(x) \\ \gamma_{\kappa 12}(x) \end{Bmatrix} = \begin{bmatrix} \frac{1-\nu_{\kappa 13}\nu_{\kappa 31}}{E_{\kappa 11}} & -\frac{\nu_{\kappa 23}\nu_{\kappa 31}+\nu_{\kappa 21}}{E_{\kappa 22}} & 0 \\ -\frac{\nu_{\kappa 13}\nu_{\kappa 32}+\nu_{\kappa 12}}{E_{\kappa 11}} & \frac{1-\nu_{\kappa 23}\nu_{\kappa 32}}{E_{\kappa 22}} & 0 \\ 0 & 0 & \frac{1}{G_{\kappa 12}} \end{bmatrix} \begin{Bmatrix} \sigma_{\kappa 11}(x) \\ \sigma_{\kappa 22}(x) \\ \tau_{\kappa 12}(x) \end{Bmatrix} + \begin{bmatrix} \alpha_{\kappa 33}\nu_{\kappa 31} + \alpha_{\kappa 11} \\ \alpha_{\kappa 33}\nu_{\kappa 32} + \alpha_{\kappa 22} \\ 0 \end{bmatrix} \Delta T \tag{1}$$

A plane stress assumption could be substituted by setting all out-of-plane Poisson terms to zero ($\nu_{\kappa 13} = \nu_{\kappa 31} = 0$). The central adherend is referred to as material a; an equilibrium element for the central adherend is pictured in Fig. 2.1. Fig. 2.2 represents the outer adherend, referred to as material c. In these two areas, x-equilibrium requires the following:

$$\begin{aligned} \frac{\partial \sigma_{a11(x)}}{\partial x} &= -\frac{2}{t_a}\tau_{b12(x)}, \\ \frac{\partial \sigma_{c11(x)}}{\partial x} &= -\frac{1}{t_c}\tau_{b12(x)}, \end{aligned} \tag{2}$$

where x is measured from the left edge of the adhesive. Solving Eqs. (2) for $\tau_{b12(x)}$ and equating leads to:

$$t_c \frac{\partial \sigma_{c11(x)}}{\partial x} = \frac{t_a}{2}\frac{\partial \sigma_{a11(x)}}{\partial x}. \tag{3}$$

The natural boundary conditions at the edge of adherend a are:

$$\begin{aligned} \sigma_{a11(0)} &= 0, \\ \sigma_{a11(l)} &= \frac{2P}{t_a}, \end{aligned} \tag{4}$$

which are the longitudinal normal stresses in the central adherend at the edges of the joint. Combining the above equations leads to the following relationship between stresses in the central and outer adherends:

$$\sigma_{c11(x)} = \frac{P}{t_c} - \frac{t_a}{2t_c}\sigma_{a11(x)}. \tag{5}$$

Since the shear stress is assumed to be constant through the thickness of the adhesive, the shear stress in the adhesive is determined by Eqs. (2) and the solution to Eq. (5). As summarized in Appendix A, Eqs. (2)–(5) can

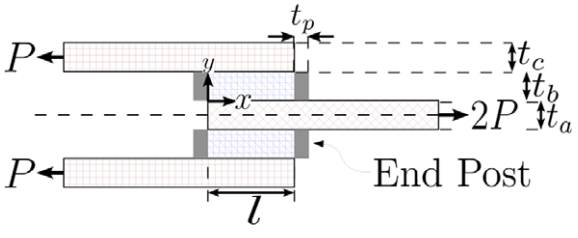

Fig. 1. Schematic of the double lap joint with end posts.

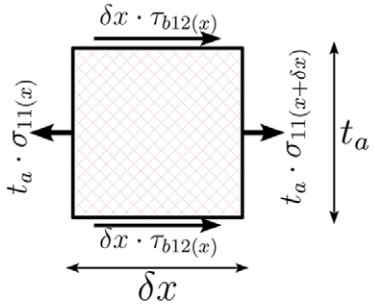

2.1: Equilibrium element of central adherend

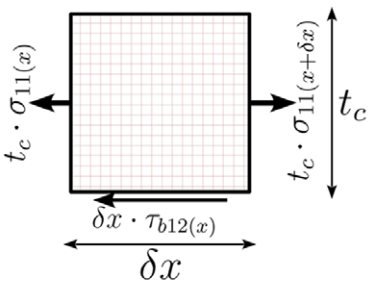

2.2: Equilibrium element of outer adherend

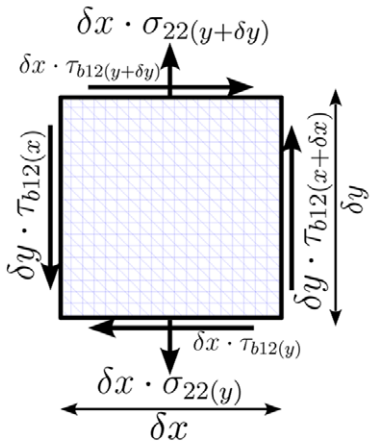

2.3: Equilibrium element of adhesive

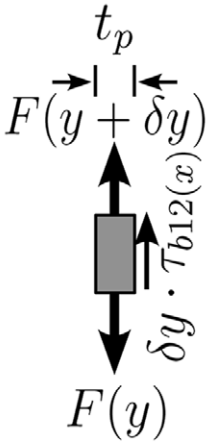

2.4: Equilibrium element of the left end post

Fig. 2. Equilibrium elements.

be combined using the principle of virtual work to solve for the central adherend stress. This leads to a differential equation in the following form:

$$\frac{\partial^2 \sigma_{a11(x)}}{\partial x^2} + \omega^2 \sigma_{a11(x)} + \psi_T + \psi_P = 0. \tag{6}$$

In Eq. (6), it is worth noting that the thermal and mechanical loads enter the differential equation in the form of system parameters ψ_T and ψ_P. Before stating the values of the system parameters ω^2,ψ_T, and ψ_P, it is reasonable to non-dimensionalize the solution to Eq. (6), therefore the following substitutions are made:

$$\begin{aligned}
\overline{\psi}_T &= \psi_T \frac{l^2}{E_{a11}}, \\
\overline{\psi}_P &= \psi_P \frac{l^2}{E_{a11}}, \\
\bar{x} &= \frac{x}{l}, \\
\overline{\omega} &= l\omega, \\
\overline{\tau}_{b12(\bar{x})} &= \frac{\tau_{b12(l\bar{x})}}{E_{a11}}, \\
\overline{\sigma}_{a11(\bar{x})} &= \frac{\sigma_{a11(l\bar{x})}}{E_{a11}}.
\end{aligned} \tag{7}$$

In Eq. (7), the non-dimensional axial stress $\overline{\sigma}_{a11(\bar{x})}$ could easily be confused for the axial strain ε_{a11}, however this is not the case since the stress field is not uniaxial. In analytical models offered previously, the average shear stress τ_{b12}^{ave} has been chosen as the normalizing factor. However, since a thermal load without an externally applied mechanical load results in a zero average shear stress, the modulus of the central adherend E_{a11} is used for the normalization. Unfortunately, this choice loses the "stress concentration factor" associated with the average shear normalization, however it is necessary to avoid a singular result for thermal loads. Upon substitution, Eq. (6) becomes:

$$\frac{\partial^2 \overline{\sigma}_{a11}}{\partial \bar{x}^2} + \overline{\omega}^2 \overline{\sigma}_{a11} + \overline{\psi}_T + \overline{\psi}_P = 0, \tag{8}$$

which is a non-dimensional form of the governing equation. The parameters $\overline{\omega}^2$, $\overline{\psi}_T$, and $\overline{\psi}_P$ are given by:

$$\begin{aligned}
\overline{\omega}^2 &= \frac{2G_{b12}l^2}{t_b}\left[\frac{(v_{c13}v_{c31}-1)}{E_{c11}t_c} + \frac{2(v_{a13}v_{a31}-1)}{E_{a11}t_a}\right], \\
\overline{\psi}_T &= \left[\frac{4G_{b12}l^2(\alpha_{c33}v_{c31} - \alpha_{a33}v_{a31} + \alpha_{c11} - \alpha_{a11})}{E_{a11}t_a t_b}\right]\Delta T, \\
\overline{\psi}_P &= -\left[\frac{4G_{b12}l^2(v_{c13}v_{c31}-1)}{E_{a11}E_{c11}t_a t_b t_c}\right]P.
\end{aligned} \tag{9}$$

It is worth noting that Eq. (9) contains non-dimensional parameters for both thermal and mechanical loading. Also, thermal expansion of the adhesive is not a factor in this model, since the adhesive is assumed to carry no longitudinal normal stress. [2]

The solution to Eq. (6) takes the form:

$$\overline{\sigma}_{a11(\bar{x})} = \bar{a}\sin(\overline{\omega}\bar{x}) + \bar{b}\cos(\overline{\omega}\bar{x}) - \frac{\overline{\psi}_T + \overline{\psi}_P}{\overline{\omega}^2}, \tag{10}$$

and possesses the following boundary conditions for longitudinal normal stress:

$$\begin{aligned}
&\overline{\sigma}_{a11}(0) = 0, \\
&\overline{\sigma}_{a11}(1) = \frac{2P}{t_a E_{a11}}.
\end{aligned} \tag{11}$$

Application of the boundary conditions leads to the following values for the coefficients $\bar{a}, \bar{b}$:

$$\begin{aligned}
\bar{a} &= -\left[\frac{E_{c11}t_b t_c}{2G_{b12}l^2\sin\overline{\omega}(v_{c13}v_{c31}-1)} + \frac{\cos\overline{\omega}-1}{\overline{\omega}^2\sin\overline{\omega}}\right]\overline{\psi}_P - \frac{(\cos\overline{\omega}-1)}{\overline{\omega}^2\sin\overline{\omega}}\overline{\psi}_T, \\
\bar{b} &= \frac{\overline{\psi}_T + \overline{\psi}_P}{\overline{\omega}^2}
\end{aligned} \tag{12}$$

and the solution is completed.

The SO solution presented in this section minimizes solution complexity. As a result, it lacks certain desirable features. It does not offer a traction free adhesive edge, nor does it quantify the peel stress. Despite these shortcomings, the model is useful. It provides an orthotropic solution which includes consideration of thermal expansion. Also, important non-dimensional parameters have been identified in Eq. (9). These parameters dictate the joint stress distribution, and can be used as a first order analysis tool in the design of bonded double lap joints. Further, the SO solution provides the foundation

[2] The assumption of zero longitudinal normal stress in the adhesive greatly simplifies the calculations, and is reasonable for calculating shear stress (and peel stress in the SP solution) as long as the strain energy due to this stress component is a small relative to the total strain energy. The model breaks down when this is not the case, such as a joint with very similar adherend thermal expansion and a large differential thermal expansion relative to the adhesive. In such cases, the longitudinal thermal stress of the adhesive will be greater than the adhesive shear stress and peel stress and a different type of analysis is appropriate.

for a formulation posed in the next section, the solution of which provides a zero traction at the adhesive edge.

3.2. A model which assumes the adhesive carries shear and peel stress

The second solution presented in this work is the SP extension to the above analysis. In this case, the adhesive is no longer confined to carry only shear stress. Instead, it is now assumed to carry shear and peel stresses, as shown in Fig. 2.3. The adherends are assumed to be stiff, and carry only normal stresses as before. For convenience, a fictitious structural element referred to as an "end post" is located at the edge of the adhesive, and is assumed to be capable of transferring any shear stress at the edge towards the adherends. In making this assumption, the traction boundary condition is satisfied a priori. This modeling approach has been used for double lap joints as described by Davies (1982), of which the current model can be considered an extension. The end post element, which is included in Fig. 1, will be carried through the calculations and then eliminated at the end to restore the correct geometry.

The stress fields in the adherends are as described in the SO solution, with the exception of the peel stress in the adhesive layer. The x-equilibrium equations provided above still hold, however, y-equilibrium in the adhesive is now included in the analysis.

Force equilibrium in the y direction of the adhesive requires the following relation:

$$\frac{\partial \sigma_{b22(x,y)}}{\partial y} = -\frac{\partial \tau_{b12(x)}}{\partial x}, \tag{13}$$

where $\sigma_{b22(y)}$ is assumed to be a linear function of y, which is the lowest order assumption that satisfies the equilibrium requirement.

$$\sigma_{b22(y)} = c_0 + c_1 y. \tag{14}$$

The peel stress at the adhesive interface is assumed to be zero, $\sigma_{b22(t_b)} = 0$, therefore:

$$\sigma_{b22(y)} = c_0\left(1 - \frac{y}{t_b}\right). \tag{15}$$

Though this assumption could be challenged, it enables y-equilibrium to be considered with a minimum of solution complexity, and is justified when the average adhesive peel stress is considered in Section (5). Combining Eq. (13) and Eq. (15) leads to:

$$\sigma_{b22(x,y)} = \frac{t_a}{2}(y - t_b)\frac{\partial^2 \sigma_{a11(x)}}{\partial x^2}. \tag{16}$$

Force equilibrium in the y direction on the left end post requires the following relation:

$$\frac{\partial F_{(y,x=0)}}{\partial y} = -\tau_{b12(0)}, \tag{17}$$

where the force carried by the end post is also assumed to be a linear function of y:

$$F_{(y,x=0)} = d_0 + d_1 y. \tag{18}$$

Combining Eq. (18) with Eqs. (2) leads to:

$$F_{(y,x=0)} = \frac{t_a}{2}\frac{\partial \sigma_{a11(x=0)}}{\partial x} y + d_0. \tag{19}$$

Using similar arguments for the right end post, and applying the equilibrium requirement that the total end post force vanishes on each side, the end post governing equations are given by Eqs. (20).

$$\begin{aligned} F_{(y,x=0)} &= \frac{t_a}{2}\frac{\partial \sigma_{a11(x=0)}}{\partial x}\left(y - \frac{t_b}{2}\right) \\ F_{(y,x=l)} &= -\frac{t_a}{2}\frac{\partial \sigma_{a11(x=l)}}{\partial x}\left(y - \frac{t_b}{2}\right) \end{aligned} \tag{20}$$

With the equilibrium requirements now complete, application of the principal of virtual forces leads to a differential equation of the following form:

$$\frac{\partial^4 \sigma_{a11(x)}}{\partial x^4} + \beta \frac{\partial^2 \sigma_{a11(x)}}{\partial x^2} + \gamma \sigma_{a11(x)} + \phi_T + \phi_P = 0. \tag{21}$$

As was the case in the SO solution, here in Eq. (21) the thermal and mechanical loads enter the differential equation in the form of system parameters ϕ_T and ϕ_P. Without explicit statement of the parameters, non-dimensionalizing substitutions can be made:

$$\begin{aligned}
\bar{x} &= \frac{x}{l}, \\
\overline{\beta} &= l^2 \beta, \\
\overline{\gamma} &= l^4 \gamma, \\
\overline{\sigma}_{a11(\bar{x})} &= \frac{\sigma_{a11(l\bar{x})}}{E_{a11}}, \\
\overline{\tau}_{b12(\bar{x})} &= \frac{\tau_{b12(l\bar{x})}}{E_{a11}}, \\
\overline{\phi}_T &= \phi_T \frac{l^4}{E_{a11}}, \\
\overline{\phi}_P &= \phi_P \frac{l^4}{E_{a11}}.
\end{aligned} \tag{22}$$

As summarized in Appendix A, the solution of Eqs. (2), (16),(20) as well as the non-dimensionalizing substitutions given in Eqs. (22) lead to the following differential equation for the normalized stress in the central adherend:

$$\frac{\partial^4 \overline{\sigma}_{a11}}{\partial \bar{x}^4} + \overline{\beta} \frac{\partial^2 \overline{\sigma}_{a11}}{\partial \bar{x}^2} + \overline{\gamma}\ \overline{\sigma}_{a11} + \overline{\phi}_T + \overline{\phi}_P = 0, \tag{23}$$

where the dimensionless system parameters are given by:

$$\begin{aligned}
\overline{\beta} &= \frac{3E_{b22}l^2}{2G_{b12}t_b^2(v_{b23}v_{b32} - 1)}, \\
\overline{\gamma} &= \frac{3E_{b22}l^4}{t_b^3(v_{b23}v_{b32} - 1)} \left[\frac{(v_{c13}v_{c31} - 1)}{E_{c11}t_c} + \frac{2(v_{a13}v_{a31} - 1)}{E_{a11}t_a} \right], \\
\overline{\phi}_T &= \left[\frac{6E_{b22}l^4(\alpha_{c33}v_{c31} - \alpha_{a33}v_{a31} + \alpha_{c11} - \alpha_{a11})}{E_{a11}t_a t_b^3(v_{b23}v_{b32} - 1)} \right] \Delta T, \\
\overline{\phi}_P &= -\left[\frac{6E_{b22}l^4(v_{c13}v_{c31} - 1)}{E_{a11}E_{c11}t_a t_b^3 t_c(v_{b23}v_{b32} - 1)} \right] P.
\end{aligned} \tag{24}$$

The solution takes the following form:

$$\overline{\sigma}_{a11}(\bar{x}) = \bar{A}e^{\bar{\lambda}_1 \bar{x}} + \bar{B}e^{-\bar{\lambda}_1 \bar{x}} + \bar{C}e^{\bar{\lambda}_3 \bar{x}} + \bar{D}e^{-\bar{\lambda}_3 \bar{x}} - \frac{\overline{\phi}_T}{\overline{\gamma}} - \frac{\overline{\phi}_P}{\overline{\gamma}}. \tag{25}$$

The bi-quadratic Eq. (25) has two dimensionless system parameters $\overline{\lambda}_1$ and $\overline{\lambda}_3$ given by Eq. (26) and presented in terms of the orthotropic material properties in Appendix C.1.

$$\overline{\lambda}^2_{[13]} = \frac{-\overline{\beta} \pm \sqrt{\overline{\beta}^2 - 4\overline{\gamma}}}{2}. \tag{26}$$

The appearance of $\overline{\beta}$ and $\overline{\gamma}$ in $\overline{\lambda}^2_{[13]}$, which in turn govern the axial stress distribution along the adherend and therefore the shear stress distribution in the adhesive (through Eqs. (13) and (16)), clearly show the relative importance of the adhesive and adherend mechanical properties and the joint geometry. Similarly, $\overline{\phi}_T$ and

$\overline{\phi}_P$ are two load parameters that are expressed through a combination of adhesive and adherend thermal and mechanical properties, loading, and joint geometry.

The coefficients $\bar{A}$, $\bar{B}$, $\bar{C}$, and $\bar{D}$ in Eq. (25) are determined by application of the boundary conditions, presented in full form in Appendix B as Eqs. (B.1) and in reduced form in Eqs. (27). These boundary conditions represent axial normal stress and shear stress at the ends of the central adherend. The reduced form is achieved by allowing the end posts to approach zero thickness (taking the limit as $t_p \to 0$). This procedure has the direct effect of forcing the shear stress at the post locations to zero, which results in a traction free surface at the adhesive edge.

$$\begin{aligned}
&\bar{D} + \bar{C} + \bar{B} + \bar{A} - \frac{\overline{\phi}_T + \overline{\phi}_P}{\overline{\gamma}} = 0 \\
&e^{-\bar{\lambda}_3}\bar{D} + e^{\bar{\lambda}_3}\bar{C} + e^{-\bar{\lambda}_1}\bar{B} + e^{\bar{\lambda}_1}\bar{A} - \frac{\overline{\phi}_T + \overline{\phi}_P}{\overline{\gamma}} - \frac{2P}{E_{a11}t_a} = 0 \\
&-\overline{\lambda}_3\bar{D} + \overline{\lambda}_3\bar{C} - \overline{\lambda}_1\bar{B} + \overline{\lambda}_1\bar{A} = 0 \\
&-\overline{\lambda}_3 e^{-\bar{\lambda}_3}\bar{D} + \overline{\lambda}_3 e^{\bar{\lambda}_3}\bar{C} - \overline{\lambda}_1 e^{-\bar{\lambda}_1}\bar{B} + \overline{\lambda}_1 e^{\bar{\lambda}_1}\bar{A} = 0
\end{aligned} \tag{27}$$

The solution of Eqs. (27) for $\bar{A}$, $\bar{B}$, $\bar{C}$, and $\bar{D}$ requires lengthy combinations of the system parameters. They are presented in a compact form in Eqs. (28), where certain repeating values have been represented as a series of multipliers μ. The values of these μ parameters are presented in Appendix C.2. With the presentation of Eqs. (28), the SP solution is now completed.

$$\begin{aligned}
\bar{A} &= \frac{\mu_{A_T}\overline{\phi}_T + (\mu_{A_T} + \mu_2\mu_3\mu_{A_P})\overline{\phi}_P}{\mu_1} \\
\bar{B} &= \frac{\mu_{B_T}\overline{\phi}_T + (\mu_{B_T} + \mu_2\mu_3\mu_{B_P})\overline{\phi}_P}{\mu_1} \\
\bar{C} &= \frac{\mu_{C_T}\overline{\phi}_T + (\mu_{C_T} + \mu_2\mu_3\mu_{C_P})\overline{\phi}_P}{\mu_1} \\
\bar{D} &= \frac{\mu_{D_T}\overline{\phi}_T + (\mu_{D_T} + \mu_2\mu_3\mu_{D_P})\overline{\phi}_P}{\mu_1}
\end{aligned} \tag{28}$$

The SP solution presented above overcomes some of the effects previously ignored in bonded joint analysis. Most significantly, it is an *orthotropic thermomechanical solution* which ensures that the shear stress at the traction free edge is zero. It does so with the minimal required complexity of a fourth order governing differential equation.

The analysis is an elastic solution, and as a result neglects the effect of adhesive and adherend plasticity, if any, on the joint. However, this effect was addressed analytically in Hart-Smith (1973a). The inclusion of plasticity effects are best treated through a numerical solution.

3.3. A dimensionless ratio of thermal and mechanical loading factors

Using the non-dimensional loading parameters defined in Eqs. (9) and (24), a dimensionless load ratio ($\overline{\phi}_{aR}$) and total load ($\overline{\phi}_{\text{total}}$) can be defined.

$$\begin{aligned}
\overline{\phi}_{aR} &= \frac{\overline{\phi}_T}{\overline{\phi}_P} = -\frac{E_{c11}t_c(\alpha_{c33}\nu_{c31} - \alpha_{a33}\nu_{a31} + \alpha_{c11} - \alpha_{a11})\Delta T}{(\nu_{c13}\nu_{c31} - 1)P} \\
\overline{\phi}_{\text{total}} &= \overline{\phi}_P + \overline{\phi}_T
\end{aligned} \tag{29}$$

The ratio $\overline{\phi}_{aR}$ is a measure of the relative importance of allowable thermal and mechanical loads. The importance of the load ratio $\overline{\phi}_{[ac]R}$ must not be underestimated. When $|\overline{\phi}_{[ac]R}| \ll 1$, mechanical stress dominates the stress field in the adherend. Conversely, when $|\overline{\phi}_{[ac]R}| \gg 1$, the thermally induced stress field is dominant. Finally, when $|\overline{\phi}_{[ac]R}| \approx 1$, thermal and mechanical loads are both significant to the total stress field. Using $\overline{\phi}_{aR}$ as

a guide, it is easy to show that some common joints, such as aluminum to carbon fiber reinforced polymer matrix composite, can be dominated by thermal loading when a large ΔT is present. It is significant that the dimensionless load ratio is the same whether the SO or the SP is used to derive it, as it is therefore independent of the adhesive stress field assumption.

The stress field that leads to the dimensionless number given in Eqs. (29) is based on the stress in the central adherend $\overline{\sigma}_{a11}(\bar{x})$. Using Eq. (5) and similarly collecting terms into dimensionless loads, a conjugate dimensionless load ratio can be written for the stress field in the outer adherend $\overline{\sigma}_{c11}(\bar{x})$:

$$\overline{\phi}_{cR} = \frac{E_{a11}t_a(\alpha_{c33}v_{c31} - \alpha_{a33}v_{a31} + \alpha_{c11} - \alpha_{a11})\Delta T}{2(v_{a13}v_{a31} - 1)P}. \tag{30}$$

Examining Eqs. (29) and (30), it is apparent that the dimensionless load ratio in one adherend depends largely on the stiffness of the other adherend.

With the dimensionless load ratio in mind, a load-based normalization can be defined by rewriting the axial stress as:

$$\overline{\overline{\sigma}}_{a11} = \frac{\overline{\sigma}_{a11}}{\overline{\phi}_{\text{total}}}, \tag{31}$$

or, more intuitively:

$$\overline{\sigma}_{a11(\bar{x})} = \overline{\overline{\sigma}}_{a11(\overline{\overline{\phi}}_P,\bar{x})} \cdot \overline{\phi}_{\text{total}}. \tag{32}$$

This second normalization can be propagated throughout the solution so that the SO and SP solutions are written as:

$$\begin{aligned} \overline{\overline{\sigma}}_{a11(\bar{x})} &= \overline{\overline{a}}\sin(\overline{\omega}\bar{x}) + \overline{\overline{b}}\cos(\overline{\omega}\bar{x}) - \frac{1}{\overline{\omega}^2}, \\ \overline{\overline{\sigma}}_{a11(\bar{x})} &= \overline{\overline{A}}e^{\overline{\lambda}_1\bar{x}} + \overline{\overline{B}}e^{-\overline{\lambda}_1\bar{x}} + \overline{\overline{C}}e^{\overline{\lambda}_3\bar{x}} + \overline{\overline{D}}e^{-\overline{\lambda}_3\bar{x}} - \frac{1}{\gamma}. \end{aligned} \tag{33}$$

Doing so requires that the boundary conditions be rewritten as:

$$\begin{aligned} &\overline{\overline{\sigma}}_{a11}(0) = 0, \\ &\overline{\overline{\sigma}}_{a11}(1) - \frac{2P}{t_a E_{a11}\overline{\phi}_{\text{total}}} = 0, \end{aligned} \tag{34}$$

for the SO solution, and for the SP solution as:

$$\begin{aligned} &\overline{\overline{D}} + \overline{\overline{C}} + \overline{\overline{B}} + \overline{\overline{A}} - \frac{1}{\overline{\gamma}} = 0, \\ &e^{-\overline{\lambda}_3}\overline{\overline{D}} + e^{\overline{\lambda}_3}\overline{\overline{C}} + e^{-\overline{\lambda}_1}\overline{\overline{B}} + e^{\overline{\lambda}_1}\overline{\overline{A}} - \frac{1}{\overline{\gamma}} - \frac{2P}{E_{a11}t_a\overline{\phi}_{\text{total}}} = 0, \\ &-\overline{\lambda}_3\overline{\overline{D}} + \overline{\lambda}_3\overline{\overline{C}} - \overline{\lambda}_1\overline{\overline{B}} + \overline{\lambda}_1\overline{\overline{A}} = 0, \\ &-\overline{\lambda}_3 e^{-\overline{\lambda}_3}\overline{\overline{D}} + \overline{\lambda}_3 e^{\overline{\lambda}_3}\overline{\overline{C}} - \overline{\lambda}_1 e^{-\overline{\lambda}_1}\overline{\overline{B}} + \overline{\lambda}_1 e^{\overline{\lambda}_1}\overline{\overline{A}} = 0. \end{aligned} \tag{35}$$

Using the load ratio $\overline{\phi}_{aR}$, we can split the coefficients into linear equations of the mechanical fraction of the load. Defining the mechanical load fraction as:

$$\overline{\overline{\phi}}_P = \frac{\overline{\phi}_P}{\overline{\phi}_{\text{total}}} = (1 + \overline{\phi}_{aR})^{-1}, \tag{36}$$

the coefficients $\overline{\overline{a}}$ and $\overline{\overline{b}}$ from Eqs. (10) for a load normalized solution can be written as:

$$\begin{aligned}\bar{\bar{a}} &= -\frac{E_{c11}t_b t_c}{2G_{b12}l^2 \sin\overline{\omega}(v_{c13}v_{c31}-1)}\overline{\overline{\phi}}_P - \frac{\cos\overline{\omega}-1}{\overline{\omega}^2\sin\overline{\omega}},\\ \bar{\bar{b}} &= \frac{1}{\overline{\omega}^2}.\end{aligned} \tag{37}$$

Similarly, the $\bar{\bar{A}}$, $\bar{\bar{B}}$, $\bar{\bar{C}}$, and $\bar{\bar{D}}$ coefficients can be written as:

$$\begin{aligned}\bar{\bar{A}} &= \frac{\mu_3\mu_{A_P}}{\mu_1\mu_2}\overline{\overline{\phi}}_P + \frac{\mu_{A_T}}{\mu_1},\\ \bar{\bar{B}} &= \frac{\mu_3\mu_{B_P}}{\mu_1\mu_2}\overline{\overline{\phi}}_P + \frac{\mu_{B_T}}{\mu_1},\\ \bar{\bar{C}} &= \frac{\mu_3\mu_{C_P}}{\mu_1\mu_2}\overline{\overline{\phi}}_P + \frac{\mu_{C_T}}{\mu_1},\\ \bar{\bar{D}} &= \frac{\mu_3\mu_{D_P}}{\mu_1\mu_2}\overline{\overline{\phi}}_P + \frac{\mu_{D_T}}{\mu_1},\end{aligned} \tag{38}$$

where the μ parameters are given in Appendix C.2. In this form, it becomes apparent that the coefficients $\bar{\bar{a}}, \bar{\bar{b}}, \bar{\bar{A}}, \bar{\bar{B}}, \bar{\bar{C}}, \bar{\bar{D}}$ (and by extension $\bar{a}$, $\bar{b}$, $\bar{A}$, $\bar{B}$, $\bar{C}$, $\bar{D}$) govern the stress distribution via the thermal and mechanical load ratio, $\overline{\phi}_{aR}$, enhancing its relevance to the study of thermomechanical loading of lap joints.

The forms presented in Eqs. (37) and (38) will allow for an iterative version of the SO or SP solution to be applied using numerical methods, when the mechanical load is dependent on the thermal load. For example, this would allow for solution of displacement constrained thermomechanical problems.

4. A finite element model for the symmetric double lap joint

To establish confidence in the SO and SP models proposed in Section (3), it is useful to compare the solution with a linear elastic FE model. Therefore, a 2D FE model has been generated for the ASTM International D 3528-96 (2002) double lap joint. An overview of the mesh is shown in Fig. 3, and the assumed geometries are given in

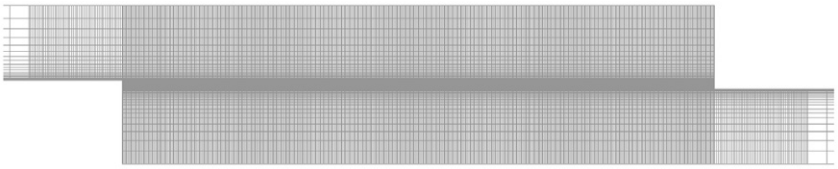

3.1: Overview of the joint section of the mesh

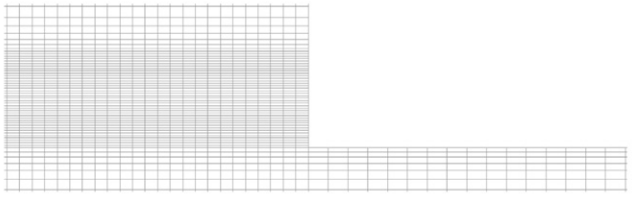

3.2: Closeup view of adhesive right edge

Fig. 3. The FE mesh.

Table 1
Geometric and loading assumptions for model comparison ASTM double lap joint geometric features (mm)

Component	Thickness	Length
Outer adherend	1.6	76.2
Adhesive	0.2 *or* 1.0	12.7
Central adherend	3.2	76.2

Table 2
Assumed loading

Load type	Value
P (N mm^{-1})	10
ΔT (°C)	10

Table 3
Assumed material properties in FE, SO, and SP solutions Assumed material properties in FE, SO, and SP solutions (moduli in GPa, expansion coeffs. in $\mu\epsilon$ °C^{-1})

Material	Aluminum	Titanium	AS4/3501-6 (0°)	FM300
E_{11}	70	110	148	1.98
E_{22}	70	110	10.6	1.98
E_{33}	70	110	10.6	1.98
G_{12}	26.3	41.4	5.61	0.71
G_{13}	26.3	41.4	5.61	0.71
G_{23}	26.3	41.4	3.17	0.71
ν_{12}	0.33	0.33	0.30	0.40
ν_{13}	0.33	0.33	0.30	0.40
ν_{23}	0.33	0.33	0.59	0.40
α_{11}	23	9	−0.8	20
α_{22}	23	9	29	20
α_{33}	23	9	29	20

Table 1. The solver used is Abaqus, and the mesh consists entirely of linear plain strain elements (CPE4). Half of the joint is modeled due to symmetry. The stress concentrations at the material interfaces are not resolved in the vicinity of the corner despite a fine mesh, since the singular stress field cannot be resolved with the FE technique used here. Loading is specified as listed in Table 2, where the mechanical load is applied far away from the lap joint and the thermal load is applied to all nodes. Displacement symmetry constraints are enforced along the mid-plane of the central adherend. Non-linear geometric stiffness is assumed.

Aluminum (Al) is used as the central adherend in all models; the outer adherends are Al, titanium (Ti), and AS4/3501-6 (AS4) Herakovich, 1998. For simplicity, the adhesive properties are assumed to be isotropic, and are estimated base on Cytec FM300 adhesive. The assumed material properties are summarized in Table 3.

Reported stresses for all models are taken from the mid plane of the adhesive. For the peel stress in the SP model, the mid-plane is the average peel stress. All peel stress comparisons are made to within 0.05 mm of the adhesive edge (25% of the adhesive thickness for the 0.20 mm adhesive models). The choice of appropriate comparison limit is complicated by the large gradients at and around the joint edge. The 0.05 mm location was chosen to be sufficiently far away from the edge so as to avoid comparison in those areas of the FE model that are dominated by the singular stress field. In those areas, the mesh dependent result has singular tensile and compressive stresses at the opposing interfaces with the adherends. In contrast, the SP predicted stress is not mesh dependent, is monotonically increasing in the comparison zone, and is well defined. Therefore, as long as the comparison limit is consistently chosen and near the edge where a strong peel stress is predicted, the magnitude of the SP predicted stress will correlate with the strength of the singularity.

5. Comparison of FE and analytical model results for ASTM lap specimens

Figs. 4–8 show the stress response predicted by the SO, SP, and FE models due thermal and mechanical loads applied to several joints. Examining the Al–Al results shown in Figs. 4.1 and 4.2, it is found that all three of the models predict that the shear and peel stress due to thermal loading is small. [3]

[3] It should be noted that this is the special case of very similar adherends subjected to primarily thermal loads. If the expansion coefficient of the adhesive was very different from that of the adherends, it would be appropriate to conduct a different type of analysis with primary focus on the adhesive expansion.

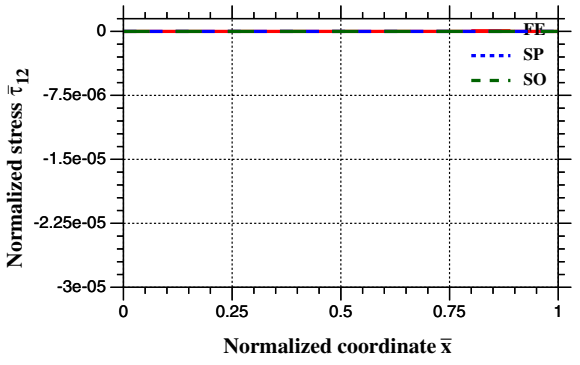

4.1: τ_{b12} due to $\bar{\phi}_T$

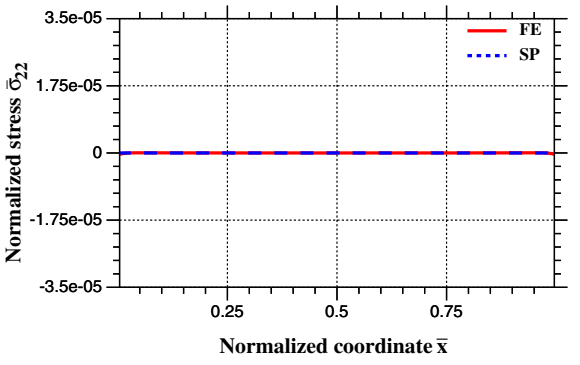

4.2: σ_{b22} due to $\bar{\phi}_T$

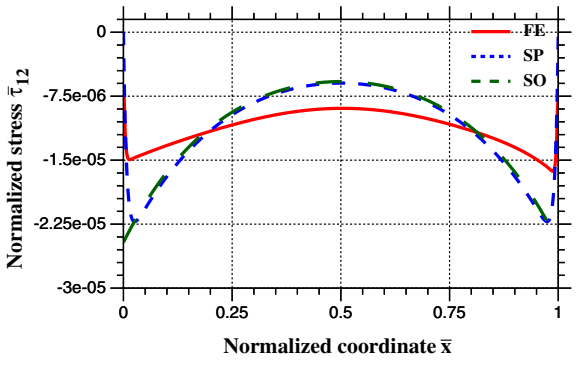

4.3: τ_{b12} due to $\bar{\phi}_P$

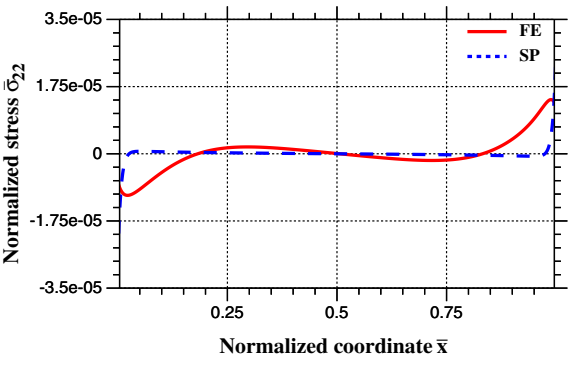

4.4: σ_{b22} due to $\bar{\phi}_P$

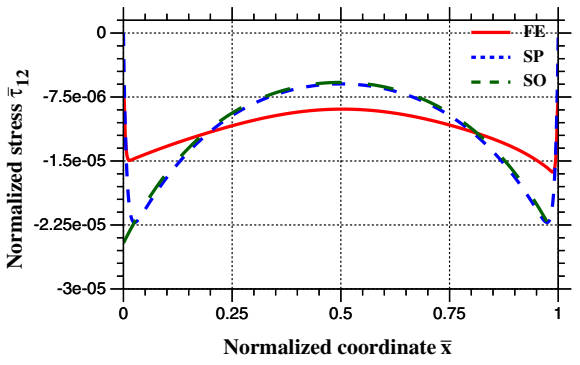

4.5: τ_{b12} due to $\bar{\phi}_P + \bar{\phi}_T$

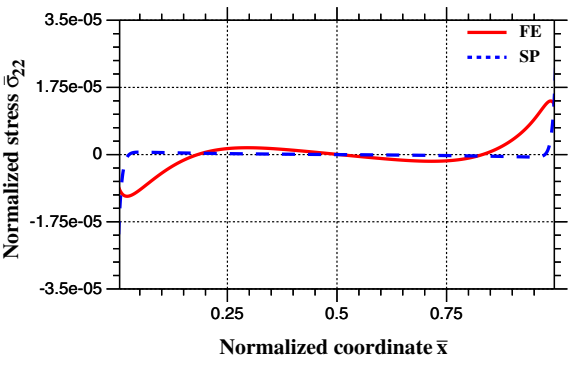

4.6: σ_{b22} due to $\bar{\phi}_P + \bar{\phi}_T$

Fig. 4. FE, SP, and SO models of Al–Al double lap joint with 0.2 mm FM300 adhesive. $\bar{\phi}_{aR} = 0$

Model predictions for an Al–Al joint with applied mechanical load are shown in Figs. 4.3 and 4.4. The first of these two figures shows the normalized shear stress $\bar{\tau}_{b12}$ in the joint. The correlation between the FE, SO, and SP models is generally good, though the SO and SP models over predict the shear stress near the edges, in comparison to the FE solution. Total shear (the area under the $\bar{x}$-$\bar{\tau}_{b12}$ curves) is preserved, because the SO and SP solutions under predict the stress in the middle of the joint relative to the FE model. The traction free boundary condition is captured by the FE and SP solutions only, as expected.

The plots in Fig. 4.4 show the peel stress due to mechanical load, as predicted by FE and SP solutions. It is apparent that differences exist in predicted peel stresses. However, near the edges of the joint, a direct correlation is found. This correlation between the two solutions at the near edge location is important, since peel

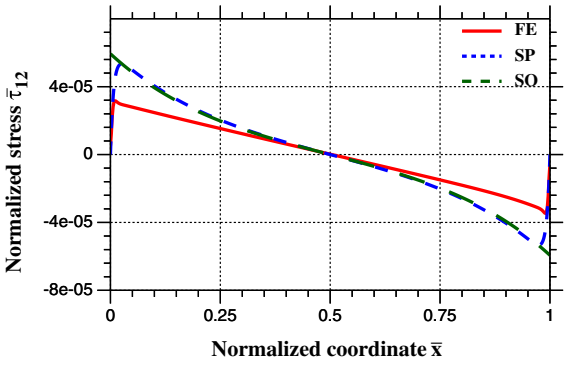

5.1: τ_{b12} due to $\bar{\phi}_T$

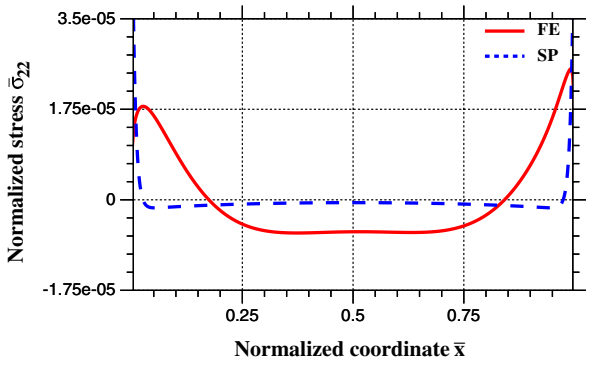

5.2: σ_{b22} due to $\bar{\phi}_T$

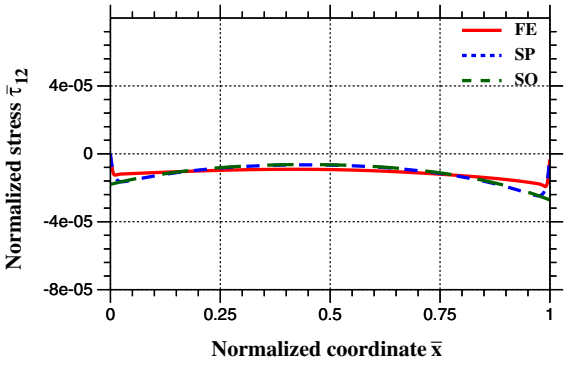

5.3: τ_{b12} due to $\bar{\phi}_P$

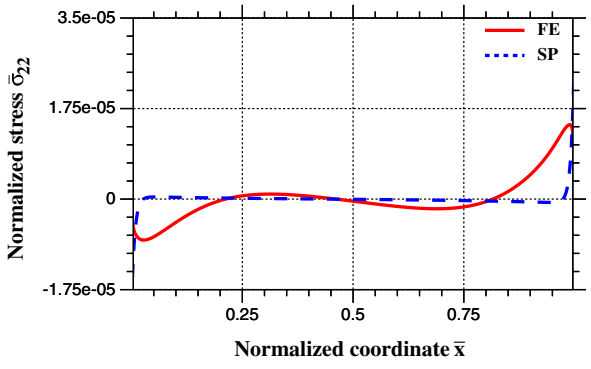

5.4: σ_{b22} due to $\bar{\phi}_P$

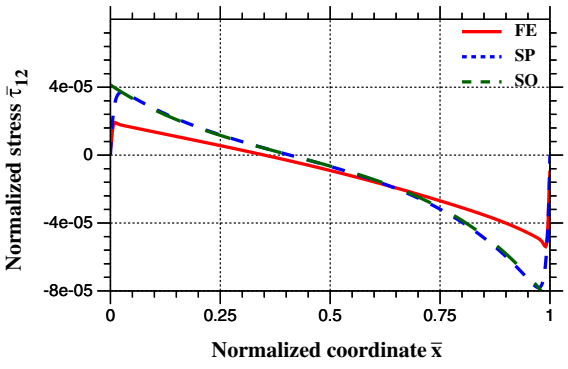

5.5: τ_{b12} due to $\bar{\phi}_P + \bar{\phi}_T$

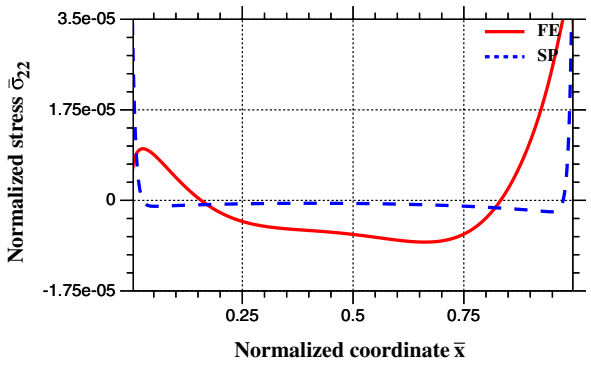

5.6: σ_{b22} due to $\bar{\phi}_P + \bar{\phi}_T$

Fig. 5. FE, SP, and SO models of Al–Ti double lap joint with 0.2 mm FM300 adhesive. $\bar{\phi}_{aR} = -3.68$

stress is often a cause of failure in lap joints. Similarly, Figs. 4.5 and 4.6 show the predicted stress state due to a mixed loading condition, where both thermal and mechanical loads are applied. In the case of the Al–Al joint, it is clear that mechanical loading dominates the stress state. This result is fully expected, since the loading ratio, $\bar{\phi}_{aR}$, is zero.

The FE, SO, and SP model predictions for Al–Ti lap joints are shown in Figs. 5 and 6. There are several observations which add confidence in the use of the derived dimensionless parameters. First, Figs. 5.1 and 6.1 show strong correlation between the FE model and the SO and SP models when thermal loading is applied to joints with differing adhesive thicknesses. The predicted shear stress is zero in the middle of the joint, which is required when there is no mechanical load. Also, the SO and SP solutions for mechanical load in Figs. 5.3 and

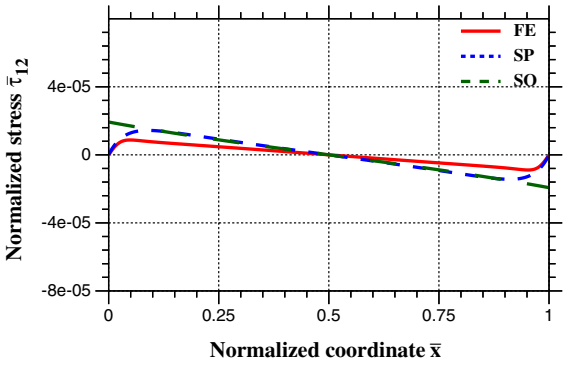

6.1: τ_{b12} due to $\bar{\phi}_T$

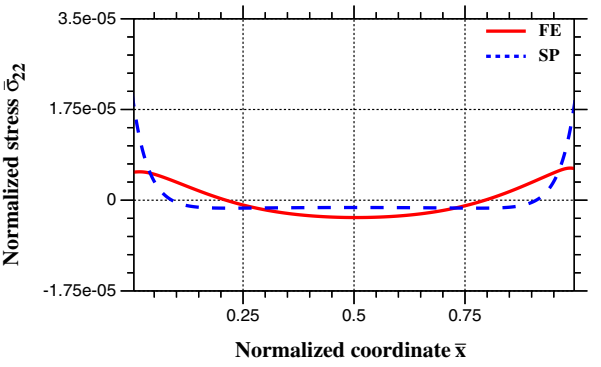

6.2: σ_{b22} due to $\bar{\phi}_T$

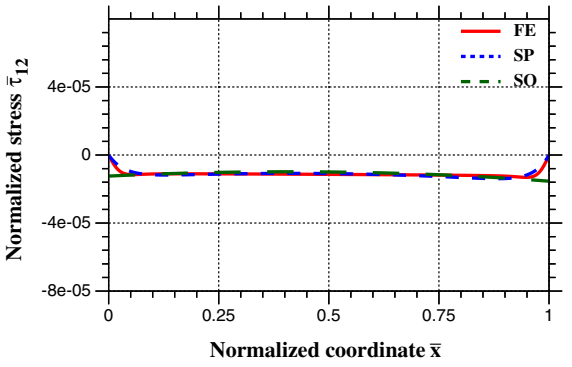

6.3: τ_{b12} due to $\bar{\phi}_P$

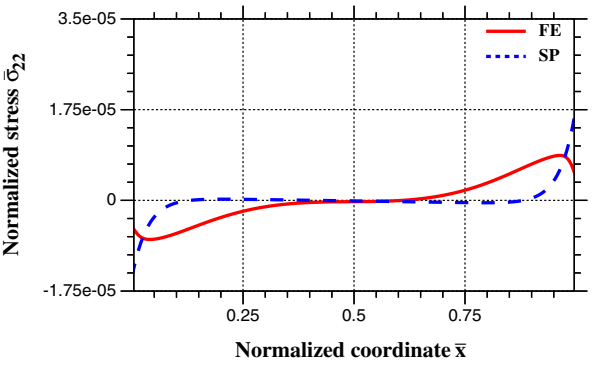

6.4: σ_{b22} due to $\bar{\phi}_P$

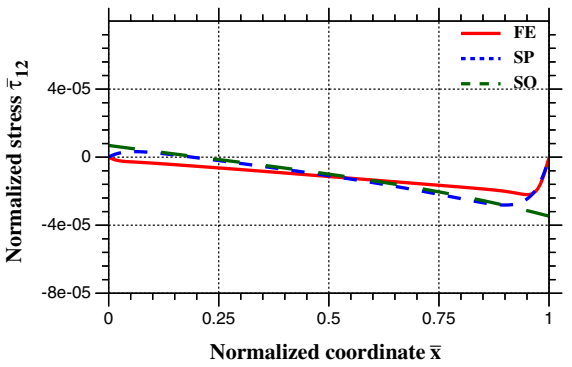

6.5: τ_{b12} due to $\bar{\phi}_P + \bar{\phi}_T$

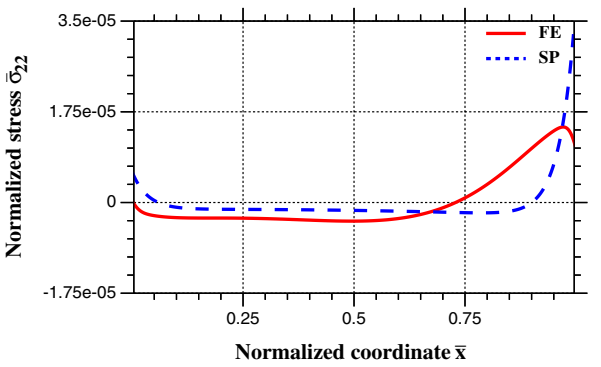

6.6: σ_{b22} due to $\bar{\phi}_P + \bar{\phi}_T$

Fig. 6. FE, SP, and SO models of Al–Ti double lap joint with 1.0 mm FM300 adhesive. $\bar{\phi}_{aR} = -3.68$

5.2 and Figs. 6.3 and 6.2 have similar correlation to the Al–Al joint. They show that the shear stress concentration at the edges is larger when the adhesive is thin than when it is thick.

Mixed loading for Al–Ti joints is shown in Figs. 5.5, 5.6 and 6.5, 6.6. These figures show that the SO and SP solutions compare well with the FE solution over the majority of the joint when the loading is thermal and mechanical. As in the Al–Al comparison, both SO and SP models tend to over predict the shear stress in the Al–TI joint, and the SP solution reasonably predicts the peel stress near the edges of the joint. Finally, comparing Figs. 5.1–5.6 and 6.1–6.6, it is shown that both the SO and SP models correlate well with the FE solution as the thickness of the adhesive is increased.

The stress predictions for the Al–AS4 joints are shown in Figs. 7 and 8, where uniaxial fiber alignment for the orthotropic AS4 is aligned with the x axis in Fig. 7, and with the z axis in Fig. 8. Though the latter is an

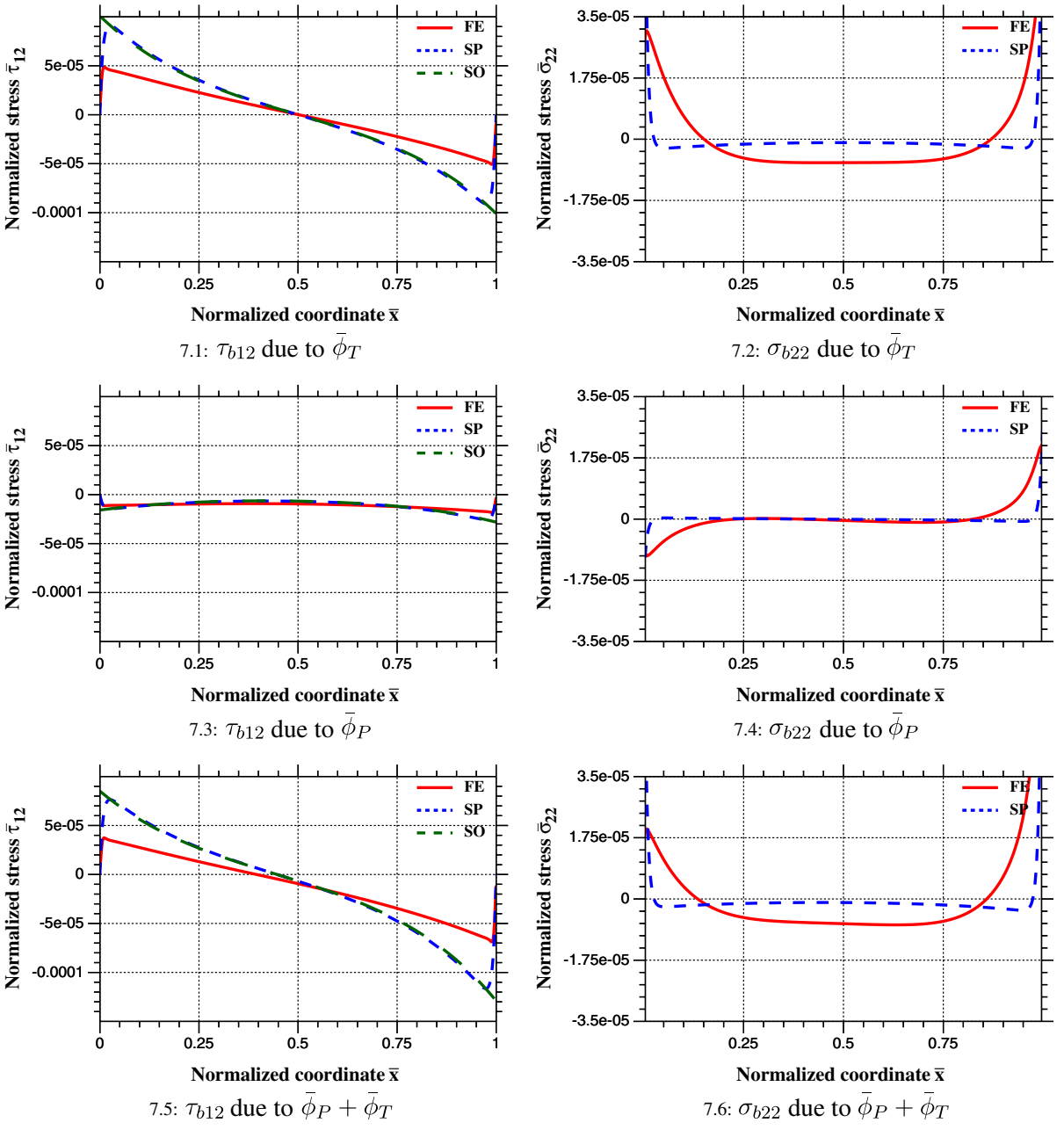

Fig. 7. FE, SP, and SO models of Al–AS4 (0°) double lap joint with 0.2 mm FM300 adhesive. $\overline{\phi}_{aR} = -7.33$

unlikely joint arrangement, it is a useful exercise to examine the orthotropic nature of the SO and SP solutions. It is immediately apparent in Figs. 7.1, 7.2 and 8.1, 8.2 that differences in the orthotropic expansion coefficients have a significant effect. The sign of the stress changes upon a 90° orientation change, and the magnitude of the stress is significantly lower as the fibers are aligned perpendicular to the cross section of the joint. This result makes sense, since the material is much more compliant when loaded in the 90° orientation.

Upon examining all predicted stress results in Figs. 4–8, the effect of the thermomechanical load ratio $\overline{\phi}_{aR}$ is apparent. The Al–Al joint, at $|\overline{\phi}_{aR}| = 0$, is dominated by mechanical load. Both Al–Ti joints, at $|\overline{\phi}_{aR}| = 3.68$, have significant contributions from both thermal and mechanical load. Comparing Al–AS4 (0°) and (90°) joints at $|\overline{\phi}_{aR}| = 7.33$ and $|\overline{\phi}_{aR}| = 0.40$, respectively, in Figs. 7 and 8, it is noted that the stress field in

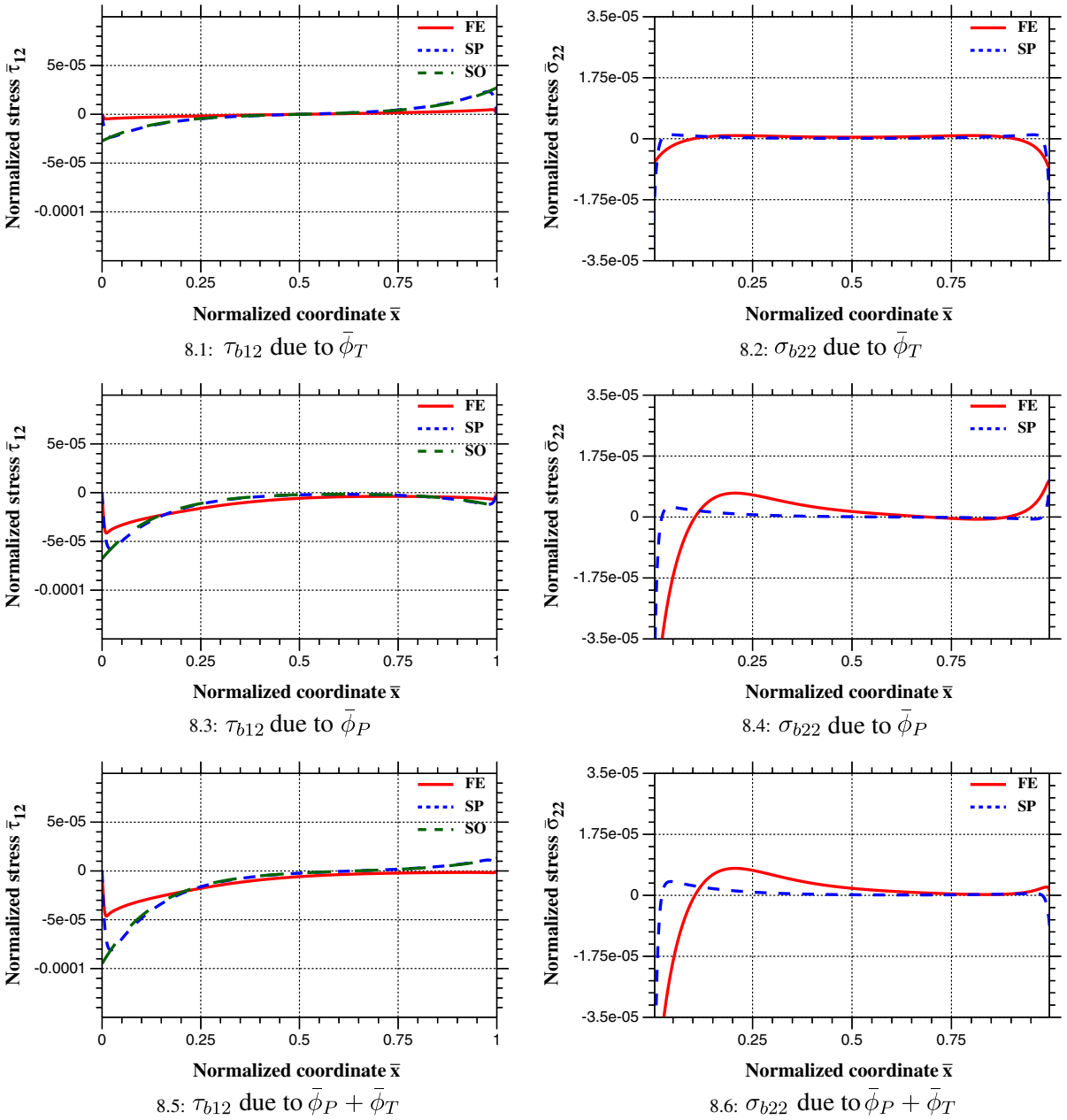

Fig. 8. FE, SP, and SO models of Al–AS4 (90°) double lap joint with 0.2 mm FM300 adhesive. $\bar{\phi}_{aR} = 0.40$

Al–AS4 (0°) lap joints is mostly due to thermal loading, whereas the stress field in Al–AS4 (90°) joint derives mostly from mechanical load. These results show the importance of $\bar{\phi}_{aR}$ in decoupling the effects of thermal and mechanical load, while the effects of $\bar{\beta}$ and $\bar{\gamma}$ are reflected in the axial and shear stress distribution in the adherend and adhesive, respectively. Further, $\bar{\phi}_{aR}$ provides a quick and effective method for determining the relative importance of thermal and mechanical loads to shear and peel stresses.

6. Concluding remarks

Two analytical models for the stress distribution in an orthotropic double lap joint have been presented with a view to identifying key non-dimensional parameters that govern joint behavior under thermo-mechan-

ical loads. The SO model assumes only shear stress exists in the adhesive, and produces a similar result to the work of Volkersen with the addition of thermal expansion. While not capturing peel stress or a traction free edge, it is a tractable solution with instructive non-dimensional parameters, and is therefore a useful tool for basic thermomechanical design of joints. The SP model, which is similar but more complex than the SO solution, does account for shear and peel stress. The 4th order governing differential equation allows for proper representation of the traction free adhesive edge. Like the SO solution, the SP solution has instructive non-dimensional parameters which can be used as tools in joint design. Unlike linear elastic FE solutions, finite stress concentrations are predicted by the SO and SP models. They can therefore be used for quick iteration in joint design as well as meaningful joint comparison based solely on constitutive material properties and joint geometry.

Non-dimensional parameters, written in terms of the joint geometry as well as the orthotropic adherend and adhesive properties, have been identified and shown to be useful in interpreting stress distribution in the joint. Two dimensionless load parameters, $\overline{\phi}_T$ and $\overline{\phi}_P$, as well as a critical dimensionless ratio, $\overline{\phi}_{aR}$ (and its conjugate parameter $\overline{\phi}_{cR}$), have been identified. These parameters control the stress distribution within the joint. It is shown that $\overline{\phi}_{aR}$, which is identically derived using either the SO or SP solutions, can be used as measure of the relative importance of mechanical and thermal loading in a joint of known (or expected) loading. The $\overline{\phi}_{aR}$ ratio allows for isolation of the thermal and mechanical portions of the solution, which will facilitate an iterative solution when the combined thermal and mechanical loads are interdependent.

Acknowledgements

This work was supported by the Space Vehicle Technology Institute under Grant NCC3-989 jointly funded by NASA and DOD within the NASA Constellation University Institutes Project, with Claudia Meyer as the project manager. P.A. Gustafson extends gratitude to all contributors to the Maxima and Octave projects, which were used for symbolic and numerical manipulations, respectively. Much of this work was completed using open source software licensed under the GNU General Public License (GPL) or one of its variants.

Appendix A. Extended description of the virtual work calculations

The principal of virtual work calculations are briefly summarized below. Equilibrium relations derived in Section (3) are given in Table 4, as well as their associated virtual stress quantities.

The adhesive peel stress distribution presented in the SP solution would require the transverse normal stress in the central adherend σ_{a22} to be included in the virtual work calculations. However, following the recommendation of Davies (1982), this addition is a secondary effect and is therefore not included in order to minimize

Table 4
Stresses and virtual stresses included in the virtual work solutions

Equilibrium stress	Virtual stress
(a) *Quantities included in the both the SO and SP models*	
$\sigma_{a11}(x)$	$\hat{\sigma}_{a11}(x)$
$\sigma_{b12}(x) = -\frac{t_a\left(\frac{\mathrm{d}}{\mathrm{d}x}\sigma_{a11}(x)\right)}{2}$	$\hat{\sigma}_{b12}(x) = -\frac{t_a\left(\frac{\mathrm{d}}{\mathrm{d}x}\hat{\sigma}_{a11}(x)\right)}{2}$
$\sigma_{c11}(x) = \frac{P}{t_c} - \frac{t_a\sigma_{a11}(x)}{2t_c}$	$\hat{\sigma}_{c11}(x) = -\frac{t_a\hat{\sigma}_{a11}(x)}{2t_c}$
(b) *Quantities included only in the SP model*	
$\sigma_{b22}(x,y) = \frac{t_a\left(\frac{\mathrm{d}^2}{\mathrm{d}x^2}\sigma_{a11}(x)\right)(y-t_b)}{2}$	$\hat{\sigma}_{b22}(x,y) = \frac{t_a\left(\frac{\mathrm{d}^2}{\mathrm{d}x^2}\hat{\sigma}_{a11}(x)\right)(y-t_b)}{2}$
$\sigma_{22_p0}(y) = \frac{t_a\left(\frac{\mathrm{d}}{\mathrm{d}x}\sigma_{a11}(x)\right)(y-t_b)}{2t_p}$	$\hat{\sigma}_{22_p0}(y) = \frac{t_a\left(\frac{\mathrm{d}}{\mathrm{d}x}\hat{\sigma}_{a11}(x)\right)(y-t_b)}{2t_p}$
$\sigma_{22_pl}(y) = -\frac{t_a\left(\frac{\mathrm{d}}{\mathrm{d}x}\sigma_{a11}(x)\right)(y-t_b)}{2t_p}$	$\hat{\sigma}_{22_pl}(y) = -\frac{t_a\left(\frac{\mathrm{d}}{\mathrm{d}x}\hat{\sigma}_{a11}(x)\right)(y-t_b)}{2t_p}$

solution complexity. In Table 4, all virtual stress quantities can be written in terms of the central adherend virtual stress $\hat{\sigma}_{a11}$. The principal of virtual work is applied using:

$$\delta W = \sum_i \int (\hat{\sigma}_i \epsilon_i) dV_i = 0, \tag{A.1}$$

where i represents the quantities listed in Table 4 for each solution. Eq. (A.1) applies for an arbitrary virtual stress $\hat{\sigma}_{a11}$. The field equations and boundary terms of the SO and SP solutions become apparent when integration of Eq. (A.1) is performed by parts.

Appendix B. Boundary conditions for the SP solution

The pre-simplified version of the longitudinal normal stress boundary conditions for the left and right edges, respectively, are:

$$\begin{aligned} &\bar{D} + \bar{C} + \bar{B} + \bar{A} - \frac{\overline{\phi}_T}{\overline{\gamma}} - \frac{\overline{\phi}_P}{\overline{\gamma}} = 0, \\ &e^{-\overline{\lambda}_3}\bar{D} + e^{\overline{\lambda}_3}\bar{C} + e^{-\overline{\lambda}_1}\bar{B} + e^{-\overline{\lambda}_1}\bar{A} - \frac{\overline{\phi}_T}{\overline{\gamma}} - \frac{\overline{\phi}_P}{\overline{\gamma}} - \frac{2P}{E_{a11}t_a} = 0. \end{aligned} \tag{B.1}$$

When normalized by the total load $\overline{\phi}_{\text{total}}$, the normal stress boundary conditions become:

$$\begin{aligned} &\bar{D} + \bar{C} + \bar{B} + \bar{A} - \frac{1}{\overline{\gamma}} = 0, \\ &e^{-\overline{\lambda}_3}\bar{D} + e^{\overline{\lambda}_3}\bar{C} + e^{-\overline{\lambda}_1}\bar{B} + e^{\overline{\lambda}_1}\bar{A} - \frac{1}{\overline{\gamma}} - \frac{2P}{E_{a11}t_a\overline{\phi}_{\text{total}}} = 0. \end{aligned} \tag{B.2}$$

The pre-simplified version of the shear stress at the edges can be represented in either case by:

$$\begin{aligned} &\frac{3\alpha_{b33}E_{b22}l^4\nu_{b32}\Delta T}{E_{a11}t_at_b\nu_{b23}\nu_{b32} - E_{a11}t_at_b} + \frac{3\alpha_{b22}E_{b22}l^4\Delta T}{E_{a11}t_at_b\nu_{b23}\nu_{b32} - E_{a11}t_at_b} \\ &\quad + \frac{(E_{p^0}l^2\overline{\lambda}_3^2t_p\nu_{b23}\nu_{b32} - E_{p^0}l^2\overline{\lambda}_3^2t_p + E_{b22}l^3\overline{\lambda}_3)\bar{D}}{E_{p^0}t_p\nu_{b23}\nu_{b32} - E_{p^0}t_p} \\ &\quad + \frac{(E_{p^0}l^2\overline{\lambda}_3^2t_p\nu_{b23}\nu_{b32} - E_{p^0}l^2\overline{\lambda}_3^2t_p - E_{b22}l^3\overline{\lambda}_3)\bar{C}}{E_{p^0}t_p\nu_{b23}\nu_{b32} - E_{p^0}t_p} \\ &\quad + \frac{(E_{p^0}l^2\overline{\lambda}_1^2t_p\nu_{b23}\nu_{b32} - E_{p^0}l^2\overline{\lambda}_1^2t_p + E_{b22}l^3\overline{\lambda}_1)\bar{B}}{E_{p^0}t_p\nu_{b23}\nu_{b32} - E_{p^0}t_p} \\ &\quad + \frac{(E_{p^0}l^2\overline{\lambda}_1^2t_p\nu_{b23}\nu_{b32} - E_{p^0}l^2\overline{\lambda}_1^2t_p \times E_{b22}l^3\overline{\lambda}_1)\bar{A}}{E_{p^0}t_p\nu_{b23}\nu_{b32} - E_{p^0}t_p} = 0, \\ &\frac{3\alpha_{b33}E_{b22}l^4\nu_{b32}\Delta T}{E_{a11}t_at_b\nu_{b23}\nu_{b32} - E_{a11}t_at_b} + \frac{3\alpha_{b22}E_{b22}l^4\Delta T}{E_{a11}t_at_b\nu_{b23}\nu_{b32} - E_{a11}t_at_b} \\ &\quad + \frac{(E_{p^l}l^2\overline{\lambda}_3^2e^{-\overline{\lambda}_3}t_p\nu_{b23}\nu_{b32} - E_{p^l}l^2\overline{\lambda}_3^2e^{-\overline{\lambda}_3}t_p + E_{b22}l^3\overline{\lambda}_3e^{-\overline{\lambda}_3})\bar{D}}{E_{p^l}t_p\nu_{b23}\nu_{b32} - E_{p^l}t_p} \\ &\quad + \frac{(E_{p^l}l^2\overline{\lambda}_3^2e^{\overline{\lambda}_3}t_p\nu_{b23}\nu_{b32} - E_{p^l}l^2\overline{\lambda}_3^2e^{\overline{\lambda}_3}t_p - E_{b22}l^3\overline{\lambda}_3e^{\overline{\lambda}_3})\bar{C}}{E_{p^l}t_p\nu_{b23}\nu_{b32} - E_{p^l}t_p} \\ &\quad + \frac{(E_{p^l}l^2\overline{\lambda}_1^2e^{-\overline{\lambda}_1}t_p\nu_{b23}\nu_{b32} - E_{p^l}l^2\overline{\lambda}_1^2e^{-\overline{\lambda}_1}t_p + E_{b22}l^3\overline{\lambda}_1e^{-\overline{\lambda}_1})\bar{B}}{E_{p^l}t_p\nu_{b23}\nu_{b32} - E_{p^l}t_p} \\ &\quad + \frac{(E_{p^l}l^2\overline{\lambda}_1^2e^{\overline{\lambda}_1}t_p\nu_{b23}\nu_{b32} - E_{p^l}l^2\overline{\lambda}_1^2e^{\overline{\lambda}_1}t_p - E_{b22}l^3\overline{\lambda}_1e^{\overline{\lambda}_1})\bar{A}}{E_{p^l}t_p\nu_{b23}\nu_{b32} - E_{p^l}t_p} = 0. \end{aligned} \tag{B.3}$$

Appendix C. Definition of the solution parameters

C.1. System parameters $\overline{\lambda}_{[13]}$ in terms of the orthotropic material properties

$$\overline{\lambda}^2_{[13]} = \frac{\pm\sqrt{\dfrac{9E^2_{b22}l^4}{4G^2_{b12}t^4_b(v_{b23}v_{b32}-1)^2} - \dfrac{12E_{b22}l^4(E_{a11}t_a v_{c13}v_{c31} + 2E_{c11}t_c v_{a13}v_{a31} - 2E_{c11}t_c - E_{a11}t_a)}{E_{a11}E_{c11}t_a t^3_b t_c(v_{b23}v_{b32}-1)}}}{2} - \frac{3E_{b22}l^2}{4G_{b12}t^2_b(v_{b23}v_{b32}-1)}. \tag{C.1}$$

C.2. μ parameters for the SP solution coefficients

The μ values of Eqs. (28) and (38) are given by:

$$\begin{aligned}
\mu_{A_T} &= \frac{\overline{\lambda}_3(e^{\overline{\lambda}_3}-1)}{\overline{\gamma}}\\
\mu_{B_T} &= \frac{e^{\overline{\lambda}_1}\overline{\lambda}_3(e^{\overline{\lambda}_3}-1)}{\overline{\gamma}}\\
\mu_{C_T} &= -\frac{\overline{\lambda}_1(e^{\overline{\lambda}_1}-1)}{\overline{\gamma}}\\
\mu_{D_T} &= -\frac{\overline{\lambda}_1(e^{\overline{\lambda}_1}-1)e^{\overline{\lambda}_3}}{\overline{\gamma}}\\
\mu_{A_P} &= -(\overline{\lambda}_3 e^{2\overline{\lambda}_3+\overline{\lambda}_1} - \overline{\lambda}_1 e^{2\overline{\lambda}_3+\overline{\lambda}_1} + 2\overline{\lambda}_1 e^{\overline{\lambda}_3} - e^{\overline{\lambda}_1}\overline{\lambda}_3 - \overline{\lambda}_1 e^{\overline{\lambda}_1})\\
\mu_{B_P} &= e^{\overline{\lambda}_1}(-2\overline{\lambda}_1 e^{\overline{\lambda}_3+\overline{\lambda}_1} + \overline{\lambda}_3 e^{2\overline{\lambda}_3} + \overline{\lambda}_1 e^{2\overline{\lambda}_3} - \overline{\lambda}_3 + \overline{\lambda}_1)\\
\mu_{C_P} &= \frac{\overline{\lambda}_1(\overline{\lambda}_3 e^{\overline{\lambda}_3+2\overline{\lambda}_1} - \overline{\lambda}_1 e^{\overline{\lambda}_3+2\overline{\lambda}_1} + \overline{\lambda}_3 e^{\overline{\lambda}_3} + \overline{\lambda}_1 e^{\overline{\lambda}_3} - 2e^{\overline{\lambda}_1}\overline{\lambda}_3)}{\overline{\lambda}_3}\\
\mu_{D_P} &= -\frac{\overline{\lambda}_1 e^{\overline{\lambda}_3}(2\overline{\lambda}_3 e^{\overline{\lambda}_3+\overline{\lambda}_1} - e^{2\overline{\lambda}_1}\overline{\lambda}_3 - \overline{\lambda}_3 - \overline{\lambda}_1 e^{2\overline{\lambda}_1} + \overline{\lambda}_1)}{\overline{\lambda}_3}\\
\mu_1 &= \overline{\lambda}_3 e^{\overline{\lambda}_3+\overline{\lambda}_1} - \overline{\lambda}_1 e^{\overline{\lambda}_3+\overline{\lambda}_1} + \overline{\lambda}_3 e^{\overline{\lambda}_3} + \overline{\lambda}_1 e^{\overline{\lambda}_3} - e^{\overline{\lambda}_1}\overline{\lambda}_3 - \overline{\lambda}_3 - \overline{\lambda}_1 e^{\overline{\lambda}_1} + \overline{\lambda}_1\\
\mu_2 &= \overline{\lambda}_3 e^{\overline{\lambda}_3+\overline{\lambda}_1} - \overline{\lambda}_1 e^{\overline{\lambda}_3+\overline{\lambda}_1} - \overline{\lambda}_3 e^{\overline{\lambda}_3} - \overline{\lambda}_1 e^{\overline{\lambda}_3} + e^{\overline{\lambda}_1}\overline{\lambda}_3 - \overline{\lambda}_3 + \overline{\lambda}_1 e^{\overline{\lambda}_1} + \overline{\lambda}_1\\
\mu_3 &= \frac{E_{c11}\overline{\lambda}_3 t^3_b t_c(v_{b23}v_{b32}-1)}{3E_{b22}l^4(v_{c13}v_{c31}-1)}.
\end{aligned} \tag{C.2}$$

References

Adams, R.D., Coppendale, J., Mallick, V., Al-Hamdan, H., 1992. The effect of temperature on the strength of adhesive joints. International Journal of Adhesion and Adhesives 12 (3), 185–190.

Adams, R.D., Comyn, J., Wake, W.C., 1997. Structural Adhesive Joints in Engineering. Chapman & Hall, London.

Allman, D.J., 1977. A theory for elastic stresses in adhesive bonded lap joints. The Quarterly Journal of Mechanics and Applied Mathematics 30, 415.

ASTM International, ASTM D 3528-96, 2002, Standard Test Method for Strength Properties of Double Lap Shear Adhesive Joints by Tension Loading.

Bednarcyk, B.A., Zhang, J., Collier, C.S., Bansal, Y., Pindera, M.J., 2006. Analysis tools for adhesively bonded composite joints, part 1: higher-order theory. AIAA Journal 44 (1), 171–180.

Benson, N.K., 1966. Influence of stress distribution on the strength of bonded joints. In: Adhesion: Fundamentals and Practice: A Report of an International Conference held at the University of Nottingham, England, 20–22 September 1966, Ministry of Technology, United Kingdom.

Chen, W.T., Nelson, C.W., 1979. Thermal stress in bonded joints. IBM Journal of Research and Development 23, 179–188.
Davies, G.A.O., 1982. Virtual Work in Structural Analysis. John Wiley & Sons, New York.
Delale, F., Erdogan, F., Aydinoglu, M.N., 1981. Stresses in adhesively bonded joints: a closed-form solution. Journal of Composite Materials 15, 249–271.
Erdogan, F., Ratwani, M., 1971. Stress distribution in bonded joints. Journal of Composite Materials 5, 378–393.
Gilibert, Y., Rigolot, A., 1988. Determination of stress distribution in double-lap joints, matched asymptotic expansions and conformal mapping. Adhesively Bonded Joints: Testing, Analysis, and Design, vol. ASTM STP 981, American Society for Testing and Materials, Philadelphia, pp. 145–159.
Goland, M., Reissner, E., 1944. The stresses in cemented joints. Journal of Applied Mechanics 66, A-17–A-27.
Hart-Smith, L.J., 1973a Adhesive-bonded double-lap joints. NASA Contractor Report 112235.
Hart-Smith, L.J., 1973b Adhesive-bonded single-lap joints. NASA Contractor Report 112236.
Her, S-C., 1999. Stress analysis of adhesively-bonded lap joints. Composite Structures 47 (1–4), 673–678.
Herakovich, C.T., 1998. Mechanics of Fibrous Composites. John Wiley and Sons, Inc., New York.
Kilic, B., Madenci, E., Ambur, D.R., 2004 Global-local finite element analysis of bonded single-lap joints. In: 45th AIAA/ASME/ASCE/AHS/ASC Structures, Structural Dynamics and Materials Conference, April 19–22, Palm Springs, CA.
Mendels, D.-A., Page, S.A., Leterrier, Y., Manson, J.-A.E. 2000. A modified double lap-shear test as a mean to measure intrinsic properties of adhesive joints. In: European Conference on Composite Materials, June 4–7, Brighton, United Kingdom.
Mortensen, F., Thomsen, O.T., 2002a. Coupling effects in adhesive bonded joints. Composite Structures 56 (2), 165–174.
Mortensen, F., Thomsen, O.T., 2002b. Analysis of adhesive bonded joints: a unified approach. Composites Science and Technology 62 (7–8), 1011–1031.
Peppiatt, N.A., 1974. Stress analysis of adhesive joints. PhD thesis, University of Bristol.
Renton, W.J., Vinson, J.R., 1975. The efficient design of adhesive bonded joints. Journal of Adhesion 7, 175–193.
Sen, J.K., Jones, R.M., 1980a. Stresses in double-lap joints bonded with a viscoelastic adhesive: part I. Theory and experimental corroboration. AIAA Journal 18 (10), 1237–1244.
Sen, J.K., Jones, R.M., 1980b. Stresses in double-lap joints bonded with a viscoelastic adhesive: Part II. Parametric study and joint design. AIAA Journal 18 (11), 1376–1382.
Vinson, J.R., Zumsteg, J.R., 1979. Analysis of bonded joints in composite material structures including hygrothermal effects. In: 20th AIAA/ASME/ASCE/AHS Structures, Structural Dynamics, and Materials Conference, St. Louis, MO.
Volkersen, O., 1938. Die niektraftverteilung in zugbeanspruchten mit konstanten laschenquerschritten. Luftfahrtforschung 15, 41–47.
Whitney, J.M., 1997. Stress analysis of a composite double-lap joint using higher order plate theory. In: Proceedings of the AIAA/ASME/ASCE/AHS/ASC 38th Structures, Structural Dynamics, and Materials Conference and Exhibit, April 7–10, 1997, Kissimmee, FL.
Yang, C., Huang, H., Tomblin, J.S., Sun, W., 2004. Elastic–plastic model of adhesive-bonded single-lap composite joints. Journal of Composite Materials 38 (4), 293–309.
Yarrington, P., Zhang, J., Collier, C., Bednarcyk, B.A., 2005. Failure analysis of adhesively bonded composite joints. In: Proceedings of the AIAA/ASME/ASCE/AHS/ASC 46th Structures, Structural Dynamics, and Materials Conference, April 18–21 2005, Austin, TX, No. 2006-1959. American Institute of Aeronautics and Astronautics.
Zhang, J., Bednarcyk, B.A., Collier, C., Yarrington, P., Bansal, Y., Pindera, M.J., 2005. 3D stress analysis of adhesively bonded composite joints. In: Proceedings of the AIAA/ASME/ASCE/AHS/ASC 46th Structures, Structural Dynamics, and Materials Conference, April 18–21 2005, Austin, TX, 2006–1959. American Institute of Aeronautics and Astronautics.
Zhang, J., Bednarcyk, B.A., Collier, C., Yarrington, P., Bansal, Y., Pindera, M.J., 2006. Analysis tools for adhesively bonded composite joints, part 2: Unified analytical theory. AIAA Journal 44 (8), 1709–1719.
Zhang, J., Collier, C., Bansal, Y., Bednarcyk, B.A., Pindera, M-J., 2004. Analysis of adhesively bonded composite joints using a higher-order theory. In: 45th AIAA/ASME/ASCE/AHS/ASC Structures, Structural Dynamics and Materials Conference, April 19–22, Palm Springs, CA.